

1 **A fully coupled Atmosphere-Ocean Wave modeling**  
2 **system (WEW) for the Mediterranean Sea: interactions**  
3 **and sensitivity to the resolved scales and**  
4 **mechanisms**

5

6 **P. Katsafados<sup>1</sup>, A. Papadopoulos<sup>2</sup>, G. Korres<sup>3</sup> and G. Varlas<sup>1,2</sup>**

7 [1]{Department of Geography, Harokopion University of Athens, 70 El. Venizelou  
8 Str., Athens, 17671, Greece}

9 [2]{Institute of Marine Biological Resources and Inland Waters, Hellenic Centre for  
10 Marine Research, Anavyssos, Attiki}

11 [3]{Institute of Oceanography, Hellenic Centre for Marine Research, Anavyssos,  
12 Attiki}

13 Correspondence to: P. Katsafados (pkatsaf@hua.gr)

14

15 **Abstract**

16 It is commonly accepted that there is a need for a better understanding of the factors  
17 that contribute to air-sea interactions and their feedbacks. In this context it is important  
18 to develop advanced numerical prediction systems that treat the atmosphere and the  
19 ocean as a unified system. The realistic description and understanding of the exchange  
20 processes near the ocean surface requires knowledge of the sea state and its evolution.  
21 This can be achieved by considering the sea surface and the atmosphere as a  
22 continuously cross talking dynamic system. With this in mind, this study aims to  
23 present the effort towards developing a new, high-resolution, two-way fully coupled  
24 atmosphere-ocean wave model in order to support both operational and research  
25 activities. A specific issue that is emphasized is the determination and  
26 parameterization of the air-sea momentum fluxes in conditions of extremely high and  
27 time-varying winds. Software considerations, data exchange as well as computational  
28 and scientific performance of the coupled system, so-called WEW, are also discussed.

1 In a case study of a high-impact weather and sea state event, the wind-wave  
2 parameterization scheme reduces the resulted wind speed and the significant wave  
3 height as a response to the increased aerodynamic drag over rough sea surfaces.  
4 Overall, WEW offers a more realistic representation of the momentum exchanges in  
5 the ocean wind-wave system and includes the effects of the resolved wave spectrum  
6 on the drag coefficient and its feedback on the momentum flux.

7

## 8 **1. Introduction**

9 There is a need for a better understanding of the factors that contribute to air-sea  
10 interaction mechanisms, and for the development of corresponding advanced prediction  
11 systems that treat the atmosphere and the sea as a unified system. The lack of consistent  
12 skill in present forecasting systems may be partially attributed to inadequate surface and  
13 boundary-layer formulations, and the lack of full coupling to a dynamic ocean (Chen et  
14 al., 2007). Sea waves play a key role in the exchange of momentum, heat and  
15 turbulent kinetic energy at the air-sea interface. Wind waves, while being generated  
16 by the wind, extract energy and momentum from the atmosphere and therefore the  
17 drag that is felt by the atmosphere over the oceans becomes sea-state dependent.  
18 Furthermore, ocean waves affect the mixing of heat and momentum in the upper  
19 ocean layers.

20 For a better description and understanding of the exchange processes near the ocean  
21 surface, an accurate forecast of the evolution of the sea state requires considering the  
22 coupled sea surface and atmosphere as a continuously cross-talking system.  
23 Generally, at shorter and even more at longer scales, reliable results can be obtained  
24 by considering the fluid layer surrounding Earth as a single system. This means to  
25 simulate the atmosphere and the ocean as a single fully coupled system and to  
26 construct multi-model, multi-scale integrated systems (Liu et al., 2011).

27 The development of fully coupled simulation systems between atmosphere and ocean  
28 is the “state of the art” in the evolution of numerical weather prediction models. The  
29 complex mechanism of the exchange of momentum, mass, salt condensation nuclei,  
30 latent and sensible heat between the atmosphere and the ocean has been improved by  
31 coupling the two systems. The large-scale perturbations in the general circulation of

1 atmosphere and ocean, the temporal variability of dynamical air-sea interaction and its  
2 feedbacks have already been incorporated into climate coupling systems (Battisti,  
3 1988; Philander et al., 1992; Soden and Held, 2006; Roberts and Battisti, 2011).  
4 During the last several years, the importance of coupling at regional scales has  
5 challenged the research community (Hodur et al., 2002; Lionello et al., 2003). Due to  
6 the limited spatial and temporal interaction scales between atmosphere and ocean, the  
7 direct and sufficient response between the coupled models is a substantial factor  
8 (Warner et al., 2010).

9 Coupled atmosphere-ocean wave systems generally exchange near surface wind  
10 velocity from the atmosphere to the surface wave and exchange friction velocity from  
11 the wave to the atmosphere. The modeling of the wave field allows the introduction of  
12 a sea surface roughness feedback on the momentum flux (Lionello et al., 2003).  
13 Primarily, the change of the intensity of a storm or a cyclone due to the wave and the  
14 drag coefficient variability, under strong wind conditions is a critical field of study.  
15 More specifically, the hurricane force winds increase the drag coefficient magnitude  
16 of the sea surface that leads to a decrease of the wind speed and a change in the wind  
17 direction. Generally, the feedbacks ultimately create non-linear interactions between  
18 different components and make it difficult to assess the full impact on each specific  
19 model (Warner et al., 2010).

20 During numerical experiments with an atmosphere-wave model for ten hurricanes in  
21 the western Atlantic Ocean during 1998-2003, the Charnock drag coefficient was used  
22 to approach sea surface friction at different wave evolution stages (Charnock, 1955;  
23 Moon et al., 2004). As a result, in hurricane force wind conditions (above  $33 \text{ m s}^{-1}$ ), a  
24 positive forcing is observed from the decrease in sea surface friction arising from the  
25 breaking waves. For this reason, the cyclones that had been simulated by wind-wave  
26 coupled models developed more slowly than those simulated by non-coupled models.  
27 Additionally, the maximum friction velocity and sea surface roughness were much  
28 larger than their counterparts in an uncoupled system, with the largest sea surface  
29 roughness located in areas with small wave ages and wind speeds of  $25\text{-}33 \text{ m s}^{-1}$  (Liu  
30 et al., 2011). Also, maximum low-level wind speeds were typically underestimated by  
31  $2\text{-}3 \text{ m s}^{-1}$  due to the feedback of ocean wave-induced stress. However, local  
32 differences in excess of  $7\text{-}10 \text{ m s}^{-1}$  were found in some coupled model simulations

1 (Doyle, 2002; Renault et al., 2012). In addition to these wind speed differences,  
2 significant wave height maxima were reduced by approximately 10% in the coupled  
3 simulations due to the enhanced roughness associated with the young ocean waves.

4 In a recent study three physical processes related to ocean surface waves, namely the  
5 surface stress, the turbulent kinetic energy flux from breaking waves, and the Stokes-  
6 Coriolis force are incorporated in a general circulation ocean model (Breivik et al.,  
7 2015). Experiments are done with the NEMO model in ocean-only (forced) mode and  
8 coupled to the ECMWF atmospheric and wave models. Using ocean-only integrations  
9 and experiments with a coupled system consisting of the atmospheric model IFS, the  
10 wave model ECWAM and NEMO, they demonstrated that the impact of the wave  
11 effects is particularly noticeable in the extra-tropics. Of the three processes, the  
12 modification of the sea-state dependent turbulent kinetic energy has the largest  
13 impact.

14 Following the above mentioned research, a number of agencies and institutes  
15 worldwide have employed coupled systems for their recent operational activities. The  
16 European Centre for Medium-Range Weather Forecasts (ECMWF) is the pioneer in  
17 the development and implementation of coupling systems. ECMWF developed a  
18 coupled ocean-wave-atmospheric model in order to be able to have two-way  
19 interaction, based on Janssen's (1989 and 1991) quasi-linear theory. The ocean-wave  
20 model of ECMWF (ECMWF WAM or ECWAM) is fully coupled to the Integrated  
21 Forecasting System (IFS) which is the operational global meteorological forecasting  
22 model of the ECMWF (ECMWF, 2013). The ECWAM model software has been  
23 developed over a period of 10 years (1992 to 2002) for operationally predicting over  
24 the whole globe (Janssen, 2004). The ECWAM code was originally written for global  
25 scale applications, however, it was extended to also run on smaller domains and in  
26 shallower water. The present version of the fully coupled system is consisted of the  
27 wave component with spatial resolution of 28 km while the spectrum is discretized  
28 with 36 directions and 36 frequencies and the atmospheric component which have  
29 spatial resolution of 16 km and vertical discretization of 137 vertical levels (ECMWF,  
30 2013; Diamantakis and Flemming, 2014).

31 The United States Geological Survey (USGS) operates the Coupled Ocean –  
32 Atmosphere – Wave – Sediment Transport (COAWST) Modeling System, which is

1 integrated by the Model Coupling Toolkit to exchange data fields between the ocean  
2 model ROMS, the atmosphere model WRF, the wave model SWAN, and the sediment  
3 capabilities developed as part of the Community Sediment Transport Modeling  
4 Project. (Warner et al., 2010). The Earth system model (CNRM-CM5) running  
5 operationally at Meteo-France consists of several existing models designed  
6 independently and coupled through the OASIS software (Redler et al., 2010). It  
7 includes the ARPEGE model for the atmosphere, the NEMO model for the ocean  
8 circulation, the GELATO model for sea-ice, the SURFEX model for land and the  
9 ocean-atmospheric fluxes and the TRIP model to simulate river routing and water  
10 discharge from rivers to the ocean (Voltaire et al., 2012).

11 In this context, this paper describes the strategy and approach adopted to develop a  
12 new, advanced, fully coupled atmosphere-ocean wave model for supporting the  
13 research and operational activities of the Hellenic Centre for Marine Research  
14 (HCMR). A specific issue that is emphasized is the determination, parameterization  
15 and the sensitivity of air-sea momentum fluxes in a case study involving extremely  
16 high and time-varying winds.

17

## 18 **2. Overview of modeling components of the coupled system**

19 The coupled system consists of two components: the atmospheric and the ocean-wave  
20 models of the POSEIDON system. The atmospheric component is based on the  
21 Workstation Eta non-hydrostatic limited area model (Papadopoulos et al., 2002;  
22 Janjic, 2001; Nickovic et al., 2001; Mesinger et al. 1988). The ocean-wave component  
23 is based on the fourth generation OpenMP (OMP) version of the WAM model  
24 (Monbaliu et al., 2000; Korres et al. 2011) and the resulting name of the coupled  
25 system is WEW.

### 26 **2.1 The atmospheric model**

27 The atmospheric model is based on an advanced version of the SKIRON/Eta  
28 mesoscale meteorological model which is a modified version of the Eta/NCEP model  
29 (Kallos et al., 1997; Nickovic et al., 2001; Papadopoulos et al., 2002). This version  
30 became the core of the second generation POSEIDON weather forecasting system

1 (Papadopoulos and Katsafados, 2009) and is fully parallelized to run efficiently on  
2 any parallel computer platform. It uses a two-dimensional scheme for partitioning  
3 grid-point space to Message Passing Interface (MPI) tasks. MPI is a protocol for the  
4 data exchange and synchronization between the executing tasks of a parallel job.

5 The Eta model is designed to use either the hydrostatic approximation or the non-  
6 hydrostatic correction in order to be able to resolve high resolution atmospheric  
7 processes. Eta is formulated as a grid-point model and the partial differential  
8 equations are represented by finite-difference schemes. The ETA model "native" grid  
9 is awkward to work with because the variables are on semi-staggered (e.g., the grid  
10 for wind is not the same as the grid for mass points) and non-rectangular (number of  
11 points in x-axis is not constant in respect to y-axis) grids. More specifically, in the  
12 horizontal dimension, the model is defined over the semi-staggered E grid, as shown  
13 in Fig. 1.

14 The Eta model is well-documented and detailed descriptions of its dynamics and  
15 physics components can be found in several studies (e.g., Mesinger et al., 1988;  
16 Janjic, 1994; Janjic et al., 2001, and references therein). The air-sea momentum fluxes  
17 are mainly parameterized in the surface layer scheme based on the well-established  
18 Monin-Obukhov similarity theory. It provides the lower boundary conditions for the  
19 2.5 level turbulence model and introduces the viscous sublayer for a more realistic  
20 representation of the near surface fluxes. Different viscous sublayer approaches are  
21 applied over ground and over water surfaces in the model. For this specific  
22 application, special care was taken in the calculation of the 10-meter wind. The  
23 calculations of the surface parameters within this viscous sublayer have an obvious  
24 advantage that decreases the level of uncertainty in the wind, air temperature and  
25 humidity fields near the surface.

26 **2.2 The ocean wave model**

27 The wave forecasting system is based on WAM Cycle-4 code parallelized using OMP  
28 directives. In order to reduce unrealistic energy loss at boundary points in cases where  
29 the waves propagate parallel and near the coast, the technique of Monbaliu et al.  
30 (2000) was applied wherein an alternative octant propagation coordinate system was  
31 introduced in the original WAM model code. For the octant advection scheme, eight

1 propagation directions are defined instead of four in the classical quadrant scheme.  
2 Although in terms of computational workload, the octant scheme almost doubles the  
3 CPU time required by the upwind advection quadrant scheme, it has clear advantages  
4 over other conventional schemes, especially near the coastlines (Cavaleri and Sclavo,  
5 1998).

6 The grid of the wave model for the Mediterranean and Black Seas expands over the  
7 geographical area 8°W – 42°E and 29°N – 48° N as shown in Fig.1 with a resolution  
8 of  $1/20^\circ \times 1/20^\circ$ . The bathymetric map has been constructed from ETOPO 2 data  
9 (National Geophysical Data Center, 2006. 2-minute Gridded Global Relief Data  
10 (ETOPO2) v2. National Geophysical Data Center, NOAA) using bi-linear  
11 interpolation and some degree of smoothing. In shallow areas of the two basins, local  
12 corrections were introduced based on nautical charts issued by the Hellenic Navy  
13 Hydrographic Service.

14 The Mediterranean and Black Seas wave model is a standalone model since it has no  
15 open boundary towards the Atlantic basin. This is justified in the sense that no  
16 significant swell from the Atlantic Ocean is expected to propagate into the  
17 Mediterranean basin through Gibraltar Straits. The Dardanelles and Bosphorus Straits  
18 are also considered to be closed boundaries thus no wave energy is advected between  
19 Black Sea and Marmara Sea and between the Marmara Sea and the Aegean. The  
20 model uses 24 directional bins ( $15^\circ$  directional resolution) and 30 frequency bins  
21 (ranging between 0.05Hz and 0.793Hz) to represent the wave spectra distribution. The  
22 model runs in shallow water mode without depth or current refraction.

23

### 24 **3. The theoretical background**

25 In the offline coupled mode, the atmospheric model parameterizes the momentum  
26 exchange at the air-sea interface by applying a viscous sublayer scheme (Janjic, 1994)  
27 in which, the roughness  $z_0$  over the sea surface is estimated by the formula:

$$28 \quad z_0 = \frac{a_w \cdot u_*^2}{g} \quad (1)$$

29 assuming a constant Charnock coefficient  $a_w=0.018$  throughout the simulation. In  
30 turn, the wave model receives the near surface wind components without providing

1 any feedback to the atmosphere. Therefore, no interaction takes place between the two  
2 models.

3 In parallel, the WAM model considers a wind input source function to the wave  
4 spectrum equation based on Janssen's (1989 and 1991) quasi-linear theory where the  
5 transfer of momentum from the wind to the wave field depends simultaneously on the  
6 wind stress and the sea state itself. Hence, the WAM model includes a set of  
7 diagnostic equations for modeling the sea surface roughness feedback on the near  
8 surface atmospheric boundary layer (Janssen, 1989). The spatial and temporal  
9 variability of the Charnock coefficient is estimated at each WAM timestep by

$$10 \quad a_w = \frac{0.01}{\sqrt{1 - \tau_w / \tau}} \quad (2)$$

11 In Eq. (2)  $\tau_w$  is the wave induced stress given by

$$12 \quad \tau_w = \rho_w g \int \frac{k}{\omega} \cdot S_{in} \cdot d\omega d\theta \quad (3)$$

13 The wave induced stress is mainly determined by the high frequency part of the wave  
14 spectrum consisting of the waves that have the largest growth rate due to the wind. In  
15 Eq. (3)  $\rho_w$  is the density of sea water,  $g$  is the gravitational acceleration,  $S_{in}$  represents  
16 the wind input term in the wave model,  $\omega$  is the angular frequency,  $\theta$  is the  
17 propagation direction and  $k$  is the wavenumber. The total stress  $\tau$  is estimated as

$$18 \quad \tau = \rho_a \cdot C_D \cdot U_{ref}^2 \quad (4)$$

19 where  $\rho_a$  is the density of air,  $U_{ref}$  is the wind speed at a reference height and  $C_D$  is  
20 the drag coefficient equals to

$$21 \quad C_D = \left( \frac{\kappa}{\log(z_{ref} / z_0)} \right)^2 \quad (5)$$

22 with  $\kappa$  being the von Karman constant. Combining Eq. (4) and Eq. (5) the total stress  
23 is given by

$$24 \quad \tau = \left( \frac{\kappa \cdot U_{ref}}{\log(z_{ref} / z_0)} \right)^2 \quad (6)$$

1 The estimated sea surface roughness length is

$$2 \quad z_0 = \frac{0.01 \cdot \tau}{\rho_a \cdot g \cdot \sqrt{1 - \tau_w / \tau}} \quad (7)$$

3 Finally, the computed friction velocity

$$4 \quad u_* = \sqrt{\tau / \rho_a} \quad (8)$$

5 is applied in the wind input source function  $S_{in}$ .

6 Therefore, in the fully coupled mode, WAM can provide the atmospheric model with  
 7 consistent values of the Charnock coefficient, roughness and the friction velocity at  
 8 each timestep. In the current version of WEW, the atmospheric model applies the  
 9 variable Charnock parameter  $a_w$  in Eq. (1) for the estimation of the sea surface  
 10 roughness length. According to the Mellor-Yamada-Janjic (MYJ) surface layer  
 11 parameterization scheme (Janjic, 1994), a viscous sublayer is assumed over the  
 12 oceans and operates under three sea state regimes: (i) smooth and transitional, (ii)  
 13 rough, and (iii) rough with spray, depending on the roughness Reynolds number and  
 14 finally on the friction velocity which is a monotonic function of  $R_r$  (Janjic, 1994)

$$15 \quad R_r = \frac{z_0 u_*}{\nu} \quad (9)$$

16 where  $\nu = 1.5 \cdot 10^{-5} \text{ m}^2 \text{ s}^{-1}$  is the kinematic viscosity of the air (Fig. 2). Then, the  
 17 estimated friction velocity from WAM is applied for the determination of the sea state  
 18 regimes, instead of the friction velocity that is computed by the atmospheric model. In  
 19 particular, the changes of the regimes have been set to  $u_{*r} = 0.3 \text{ ms}^{-1}$  and  $u_{*s} = 0.7 \text{ ms}^{-1}$ .

20 The friction velocity of the atmospheric model is then estimated by

$$21 \quad u_* = \left[ \left( \frac{K_{Msfc}}{\Delta z_e} \right) (U_{LM} - U_{z_U}) \right]^{1/2} \quad (10)$$

22 where  $K_{Msfc}$  is the Mellor-Yamada level 2 discrete momentum exchange coefficient,  
 23  $\Delta z_e$  is the depth of the atmospheric layer that is extended between the lowest model  
 24 level and the height of the “dynamical turbulence layer” at the bottom of the surface  
 25 layer. The final term is the scalar difference between the wind velocity estimated at  
 26 the lowest model level and the velocity at a height  $z$  above the surface where the

1 molecular diffusivities are still dominant (usually at the height of the viscous  
2 sublayer). The depth of the viscous sublayer for the momentum is estimated by

$$3 \quad z_U = \zeta v \frac{M \left( \frac{z_0 u_*}{v} \right)^{1/4}}{u_*} \quad (11)$$

4 where  $\zeta=0.50$  and  $M$  is depending on the sea state regime. For smooth regime,  $M=35$ ,  
5 and when the flow ceases to be smooth,  $M=10$ . The atmospheric roughness obtained  
6 from the Eq. (1) and the friction velocity from the Eq. (10) are then implemented for  
7 the estimation of the near surface ( $Z_{U10}=Z_U+10$ ) wind components.

8

#### 9 **4. Software considerations of the coupled system**

10 In the two-way coupled mode, the Eta and WAM models utilize different domain  
11 projections, integration time step, grid geometry and cell size. Therefore, a major  
12 effort has been undertaken in order to homogenize and handle the data exchange  
13 between the atmospheric and the ocean-wave components of the coupled system.  
14 These exchanges are built upon the MPI directives since it became a standard for  
15 developing parallel applications (Snir et al., 1998). Under the parallel environment of  
16 Multiple Program Multiple Data (MPMD), the two components are carried out as  
17 parallel tasks on different processors and they exchange information in directly (Fig.  
18 3). Thus, the parallel execution of the system is handled entirely by the  
19 `mpirun/mpiexec` commands and the two components maintain their own executables.  
20 The communication between the two models is performed using `MPI_Send` and  
21 `MPI_Recv` calls at every source time step of the ocean-wave model integration and  
22 the system runs flawlessly combining both `MPICH` and `OMP` environments. After the  
23 initial development, the modification of each component source code is relatively  
24 simple, just adding some data exchange routines and inserting the appropriate  
25 commands in the original model code which call the coupling routines, while each  
26 component keeps its original structure.

27 At the initialization stage, the atmospheric model initializes and loads the inter- and  
28 intra-communicators. The atmospheric model sends the near surface wind  
29 components to the wave model and receives the variable Charnock coefficient array,

1 which is then used for the estimation of  $z_0$  in the surface layer parameterization  
2 scheme. Each data exchange requires re-projection from the atmospheric model  
3 Arakawa-E grid to the ocean-wave model regular lat-lon grid and vice versa (Fig. 4).  
4 For consistency, the sea-masks are exchanged at the initialization stage and the  
5 atmospheric to ocean-wave timestep ratio is set to 1/24 but it can be adjusted to any  
6 other configuration through the main namelist of the system. Moreover, data  
7 exchanges can easily be expanded or eliminated and the ocean-wave outputs  
8 (significant wave height and period, Charnock coefficient, friction velocity, etc.) are  
9 finally redirected through the internal communicators as outputs of the atmospheric  
10 component.

11 The initial version (v.0) of WEW was configured on a 2x2 topology (2 additional  
12 processes are allocated for setting the I/O servers) for the atmospheric component  
13 (Fig. 5). The ocean-wave component is parallelized using OMP directives and was  
14 configured with 2 threads. The current version (v.5) has been configured with a very  
15 fine horizontal resolution of  $1/20^\circ \times 1/20^\circ$  with 493x461 E-grid points and 1001x381  
16 regular lat-lon points. Numerous tests have been performed in order to extract the  
17 optimum topology. To this end, 28 threads have been allocated in total, 20 of which  
18 are dedicated to the execution of atmospheric component while the remaining 8 are  
19 reserved for the ocean-wave component. Thus, WEW is running on a Dual Quad core  
20 Intel Xeon platform cluster using 28 threads in total at 4 nodes, but it is easily  
21 portable to other architectures and flexible enough to adopt different topologies. For  
22 the abovementioned configuration, WEW requires almost 10 minutes for each  
23 simulation hour.

24 A multi-level flowchart of the system and the data exchanges are depicted in Fig. 6. In  
25 the offline coupling mode (CTRL hereafter) the atmospheric component sends hourly  
26 near surface wind velocity to the ocean-wave model without any other interaction  
27 between the two models (red line). In the two-way fully coupled mode (WEW  
28 hereafter) the atmospheric model sends the near surface wind components at every  
29 WAM model timestep and receives various near sea surface variables. In more details,  
30 for each timestep WAM can provide the atmospheric model with consistent values of  
31 the Charnock coefficient, friction velocity, total surface stress, etc. In the current  
32 version, the atmospheric model ingests Charnock coefficient and friction velocity

1 values into the Mellor Yamada surface layer parameterization scheme for the  
2 estimation of the near surface wind components for the next timestep as well as the  
3 accurate determination of the viscous sublayer and the parameterization of the air-sea  
4 momentum fluxes.

5

## 6 **5. System configuration**

7 WEW has been configured on a domain encompasses the Mediterranean Sea and the  
8 Black Sea with a horizontal resolution of  $0.05^\circ \times 0.05^\circ$  (Fig. 7). However, various tests  
9 of the system at the initial stages of the development were performed using a coarser  
10 grid of  $0.10^\circ \times 0.10^\circ$ . Gridded data from the European Centre for Medium range  
11 Weather Forecast (ECMWF) were used as initial and boundary conditions of the  
12 atmospheric component. The grid of the wave model for the Mediterranean and Black  
13 Seas covers the geographical area  $8^\circ\text{W} - 42^\circ\text{E}$  and  $29^\circ\text{N} - 48^\circ\text{N}$  as shown in Fig. 7  
14 (black line) using resolution similar to that of the atmospheric component. The  
15 different projection of the two components yields a mismatch between the two  
16 domains. Thus, a constant Charnock coefficient  $a_w=0.018$  was implemented for the  
17 sea grid points of the atmospheric domain (near its western boundary) which were  
18 outside the WAM model domain. A 1-2-1 smoothing filter was also applied over the  
19 transition zone in order to reduce artificial generated waves. The initialization of  
20 WAM was based on a wind-sea spectrum computed on the basis of the initial wind  
21 field and was produced during the preprocessing stage of the atmospheric model (cold  
22 start).

23 Each component of WEW maintained its own timestep. The propagation timestep of  
24 the WAM model was 120 sec while its source timestep was 360 sec. The coupling  
25 procedure exchanges data on the source timestep of WAM model,  $DT_w=360$  sec. As  
26 the timestep of the atmospheric model was  $DT_a=15$  sec, the exchange took place  
27 every 24 timesteps of the atmospheric model. Every hour WEW stored its unified  
28 outputs (including atmospheric and ocean-wave fields) on the native Arakawa-E grid.  
29 The configuration of the system is summarized in Table 1.

30

## 31 **6. Application and performance of the WEW system**

1 WEW has been tested for its consistency and performance in a high-impact  
2 atmospheric and sea state case study of an explosive cyclogenesis over the Ligurian  
3 Sea. The coupling efficiency was quantitatively estimated over sea areas using  
4 traditional statistical scores. Thus, the performance of the fully two-way coupled  
5 system (WEW) was compared against its performance in the offline coupling mode  
6 (CTRL) based on a point-to-point comparison with in situ observations from a  
7 network of 39 buoys in the Mediterranean Sea (Fig. 8). The consistency of WEW was  
8 also assessed against remote sensed data retrieved from CRYOSAT, ENVISAT,  
9 ESR2 and JASON1/2.

10 The incident of 4–11 January, 2012 has been selected due to the severity of the  
11 prevailing atmospheric conditions characterized by an explosive cyclogenesis over the  
12 Ligurian Sea (Varlas et al., 2014). In more detail, on January 5, 2012 a low pressure  
13 system formed over the cyclogenetic area of the Ligurian Sea. It was mainly triggered  
14 by a widespread upper-level trough extending from Central Europe to the  
15 Mediterranean Sea (Fig. 9a). The upper-level trough rapidly intensified the system  
16 and supported its southeastern movement (Fig. 9b). **On January 6, the system moved  
17 toward the Eastern Mediterranean, where the pressure dropped more than 1 bergeron,  
18 satisfying the criteria for an explosive cyclogenesis event (Fig. 10 a and b). Sanders  
19 and Gyakum (1980), defined an extratropical cyclone as a meteorological bomb when  
20 the mean sea-level pressure of its center falls by at least 1hPa per hour for 24 hours at  
21 60°N. An equivalent rate is obtained for a latitude  $\varphi$  by multiplying this rate by the  
22 dimensionless number  $\sin\varphi/\sin60^\circ$ , which is denoted as one Bergeron (Katsafados et  
23 al., 2011).** During January 6 and 7, the strong pressure gradient provoked gale force  
24 winds and significant storm surge over a vast area, including the Central  
25 Mediterranean and the Aegean Sea. It is worth noting that the buoys in the Ligurian  
26 and Balearic Seas recorded wind speeds exceeding  $20 \text{ ms}^{-1}$  and significant wave  
27 height (SWH) over 5m.

28 The horizontal distributions of the wind speed and the SWH as well as their  
29 differences between WEW and the CTRL experiment are depicted in Fig. 11. On  
30 January 6, 2012 at 18 UTC, winds exceeding the  $22 \text{ ms}^{-1}$  and SWH over 8 m cover a  
31 large part of the Mediterranean Sea (Fig. 11a and b). The horizontal distribution of  
32 differences between WEW and the CTRL experiments reveals a systematic reduction

1 of the wind speed and the SWH in the two-way fully coupled mode (WEW). The near  
2 surface wind speed differences vary up to  $2 \text{ ms}^{-1}$  and are located over the areas where  
3 maximum wind velocities occurred (Fig. 11c). The reduced wind speed simulated by  
4 WEW, as a feedback of the enhanced sea surface roughness, impacts the estimated  
5 SWH as well (Fig. 11d). Thus, SWH differences up to 1.2 m occur over the areas of  
6 the maximum wind speed reduction (eg. the area between the Balearic and Tyrrhenian  
7 Seas). Similar results have been also observed by Doyle (2002), Liu et al. (2011) and  
8 Renault et al. (2012).

9 The outputs from both simulations, CTRL and WEW, have been statistically assessed  
10 based on a point-to-point hourly comparison between model-generated variables and  
11 the available Mediterranean buoy measurements. Hourly pairs of observed and  
12 estimated values were obtained using the nearest-neighbor interpolation technique,  
13 taking care of whether this nearest source point is a sea masked grid point. Both  
14 simulations slightly underestimate the near surface wind speed, often exceeding  $1 \text{ ms}^{-1}$   
15 <sup>1</sup>. The underestimation is more prominent for wind speeds exceeding  $8 \text{ ms}^{-1}$  (Fig.  
16 12a). Although WEW increases the underestimation, it offers an overall improvement  
17 of the RMS error by approximately 2%. Additionally, it decreases the standard  
18 deviation of the model towards the standard deviation of the buoys. In accordance  
19 with the wind speed, the bias scores of the SWH indicate an underestimation for the  
20 CTRL simulation more prominent in WEW (Fig. 12b). However, WEW offers an  
21 overall improvement of more than 7% in the SWH error, with 0.53 instead of 0.57 m,  
22 and increased correlation coefficients.

23 The systematic underestimation of the wind speed persists in the comparison against  
24 the remote sensed data referenced in this section. The WEW enhances the  
25 underestimation of CTRL but also reduces the RMSE by 1.5% (Fig. 12c). In contrast  
26 to the slight overestimation of the CTRL, WEW underestimates the SWH as well  
27 (Fig. 12d). It further improves the statistical scores and shows a RMSE decrease by  
28 almost 11%. Entire indexes are also statistically significant at the 95% confidence  
29 level. This is attributed to the fact that the application of the two-way fully coupled  
30 system can generate and support a more realistic near sea surface circulation pattern  
31 by fully resolving air-sea interaction processes at the relevant interface, including the  
32 wind speed regime and wave patterns.

## 1 **6.1 Physical interpretation**

2 The particular interactions considered in WEW are mainly driven by the momentum  
3 exchanges in the ocean wind-wave system. The fully coupled wind-wave  
4 parameterization scheme includes the effects of the resolved wave spectrum on the  
5 drag coefficient and its feedback on the momentum flux. In general, the feedbacks  
6 create non-linear interactions in the dynamic structure of a storm or a cyclone due to  
7 the time-space sea surface friction variability. In WEW simulations, the maximum  
8 friction velocity and sea surface roughness are much larger than their counterparts in  
9 CTRL, with the maxima located in areas with small wave ages and wind speeds above  
10  $20 \text{ ms}^{-1}$ . The increased near sea surface friction builds a more turbulent and deeper  
11 PBL, preventing faster evolution of the storm (Fig. 13).

12 The reduction of the near surface wind speed, as was evident in the WEW simulation  
13 and depicted in Fig. 11c, is mainly attributed to the variable Charnock coefficient  
14 directly ingested in Eq. (1) for the roughness length estimation in the MYJ surface  
15 layer parameterization scheme. In the CTRL and WEW experiments, the Charnock  
16 coefficient logarithmically increases with wind speed at approximately  $22 \text{ ms}^{-1}$  (Fig.  
17 14). The enhanced Charnock coefficient increases the roughness length and decreases  
18 the near surface wind speed in WEW simulations. This also affects the estimation of  
19 the significant wave height in the two-way coupled simulations. Especially in WEW,  
20 the saturation of the Charnock coefficient for wind speeds exceeding  $22 \text{ ms}^{-1}$  indicates  
21 that in extremely high wind conditions, the sea surface friction is preserved or even  
22 decreases, offering a positive forcing to the flow. Beyond this speed, the sea surface  
23 does not become any rougher in the aerodynamic sense. The saturation of the  
24 aerodynamic roughness, finally, leads to flow separation due to the continuous wave  
25 breaking in areas where the flow is unable to follow the wave crests and troughs  
26 (Donelan et al., 2004). This wind-wave parameterization feature offers a more  
27 realistic representation of the aerodynamic drag over rough sea surfaces. Similar  
28 findings have been also confirmed by relevant studies (eg. Bao et al., 2000; Makin  
29 2005; Chen et al., 2007).

30 The roughness length as a function of the friction velocity is characterized by an  
31 initial decrease as the surface condition goes from aerodynamically smooth to  
32 aerodynamically rougher regime (Fig. 15). This is the result of an aerodynamically

1 smooth surface where the molecular motions are dominant in the developed viscous  
2 sublayer (Csanady, 2001). In moderate and fully rough sea state regimes the  
3 roughness length is exponentially increasing with the friction velocity. The roughness  
4 length in WEW is substantially larger than in CTRL for friction velocities exceeding  
5  $0.60 \text{ ms}^{-1}$ . It also shows a tendency to saturation for friction velocities exceeding  $1 \text{ ms}^{-1}$ .  
6 This is an indication of the enhanced friction in WEW under rough sea state  
7 regimes as a result of the variable Charnock parameter in the surface layer  
8 parameterization scheme.

9

## 10 **7. Concluding remarks and future perspectives**

11 WEW is the recently developed two-way fully coupled atmosphere-ocean wave  
12 system designed to support air-sea interaction research and operational activities at  
13 HCMR. The system is built in the MPMD environment where the atmospheric and the  
14 ocean-wave components are handled as parallel tasks on different processors. In the  
15 offline coupled mode, the atmospheric component parameterizes the air-sea  
16 momentum by estimating the roughness length over the sea surface as a function of a  
17 constant Charnock coefficient throughout the simulation. The ocean-wave component  
18 passively receives the near surface wind components and there is no interaction  
19 between the two models. In WEW, the atmospheric model sends the near surface  
20 wind components to the wave model on its timestep frequency and receives the space-  
21 time variable Charnock field, which is directly applied in the surface layer  
22 parameterization scheme for the estimation of the roughness length.

23 Interactions considered in WEW are mainly driven by the momentum exchanges in  
24 the ocean wind-wave system and include the effects of the resolved wave spectrum on  
25 the drag coefficient and its feedback on the momentum flux. As a general outcome,  
26 the maximum friction velocity and sea surface roughness are much larger than their  
27 counterparts in the offline coupled mode, which resulted in a more turbulent and  
28 deeper marine PBL. The reduction of the near surface wind speed in the fully coupled  
29 simulation is mainly attributed to the enhanced Charnock coefficient which increases  
30 the roughness length and finally decreases the SWH. The Charnock coefficient  
31 logarithmically increases with wind speed at approximately  $22 \text{ ms}^{-1}$  and the saturation  
32 above indicates that in extremely high wind conditions the sea surface friction is

1 preserved or even decreases, resulting a positive forcing to the flow. This wind-wave  
2 parameterization feature offers a more realistic representation of the aerodynamic  
3 drag over rough sea surfaces (Chen et al., 2007).

4 This aspect was tested in a high-impact atmospheric and sea state case study of an  
5 explosive cyclogenesis in the Mediterranean Sea. Despite the increased  
6 underestimation, affecting both wind speed and significant wave height, WEW offers  
7 an overall improvement in their RMS error up to 11%. The underestimation is  
8 attributed to the direct implementation of the variable Charnock coefficient in the  
9 current surface layer parameterization scheme and is more prominent at gale force  
10 wind speeds. Therefore, an extended modification of the current MYJ scheme is  
11 recommended, and it is in the authors' future plans, in order to adjust it to the updated  
12 sea surface forcing dynamically obtained from the ocean-wave component. To this  
13 end, an alternative parameterization scheme is under development for the more  
14 realistic representation of the sea surface momentum exchange and its feedbacks in  
15 WEW.

16

17 **Code availability**

18 For ETA model and WAM model users, the relevant code modifications for coupling  
19 the two numerical systems can be made available by Prof. Petros Katsafados  
20 ([pkatsaf@hua.gr](mailto:pkatsaf@hua.gr)), Dr. Anastasios Papadopoulos ([tpapa@hcmr.gr](mailto:tpapa@hcmr.gr)) and Dr. Gerasimos  
21 Korres ([gkorres@hcmr.gr](mailto:gkorres@hcmr.gr)).

22

23 **Acknowledgments**

24 This research is supported by the EU-funded project MyWave (FP7-SPACE-2011-  
25 1/CP-FP, SPA.2011.1.5-03). ISPRA and IFREMER (Globwave project) are gratefully  
26 acknowledged for the provision of buoy and satellite data respectively. ECMWF is  
27 also acknowledged for the kind provision of the gridded analyses data.

28

29

30

1

## 2 **References**

3 Bao, J. W., Wilczak, J. M., Choi, J. K. and Kantha, L. H.: Numerical simulations of  
4 air-sea interaction under high wind conditions using a coupled model: a study of  
5 hurricane development, *Mon. Wea. Rev.*, 128, 2190-2210, 2000.

6 Battisti, D. S.: Dynamics and thermodynamics of a warming event in a coupled  
7 tropical atmosphere-ocean model, *J. Atmos. Sci.*, 45(20), 2889-2919, 1988.

8 Breivik, Ø., K. Mogensen, J.-R. Bidlot, M. A. Balmaseda, and P. A. E. M. Janssen,  
9 *Surface wave effects in the NEMO ocean model: Forced and coupled experiments*, *J.*  
10 *Geophys. Res. Oceans*, 120, 2973–2992, doi:10.1002/2014JC010565.

11 Cavaleri, L., and Sclavo, M.: Characteristics of quadrant and octant advection  
12 schemes in wave models, *Coastal Engineering*, 34, 3-4, 221-242, 1998.

13 Charnock, H.: Wind stress on a water surface, *Quart. J. Roy. Meteor. Soc.*, 81(350),  
14 639-640, 1955.

15 Chen, S. S., Zhao, W., Donelan, M. A., Price, J. F., and Walsh, E. J.: The CBLAST-  
16 Hurricane Program and the Next-Generation Fully Coupled Atmosphere-Wave-Ocean  
17 Models for Hurricane Research and Prediction, *Bull. Amer. Meteor. Soc.*, 88, 311-  
18 317, 2007.

19 Csanady, G. T.: Air-sea interaction: Laws and mechanisms. Cambridge University  
20 Press, ISBN 0521796806, pp. 249, 2001.

21 Diamantakis, M., and Flemming, J.: Global mass fixer algorithms for conservative  
22 tracer transport in the ECMWF model, *Geosci. Model Dev.*, 7(3), 965-979, 2014.

23 Donelan, M. A., Haus, B. K., Reul, N., Plant, W. J., Stiassnie, M., Graber, H. C.,  
24 Brown, O. B., Saltzman, E. S.: On the limiting aerodynamic roughness of the ocean in  
25 very strong winds, *Geophys. Res. Lett.*, 31, 4539-4542, 2004.

26 Doyle, J. D.: Coupled atmosphere-ocean wave simulations under high wind  
27 conditions, *Mon. Wea. Rev.*, 130(12), 3087-3099, 2002.

28 *IFS Documentation, Part VII: ECMWF wave model, 2013:*  
29 <http://old.ecmwf.int/research/ifsdocs/CY40r1/>, last access: 19 August 2015.

30 Hodur, R. M., Pullen, J., Cummings, J., Hong, X., Doyle, J. D., Martin, P., and  
31 Rennick, M. A.: The Coupled Ocean/Atmosphere Mesoscale Prediction System  
32 (COAMPS), *Oceanography*, 15(1), 88–98, 2002.

33 Janjić, Z. I.: The step-mountain eta coordinate model: further developments of the  
34 convection, viscous sublayer, and turbulence closure schemes, *Mon. Wea. Rev.*, 122,  
35 927–945, 1994.

36 Janjic, Z. I., Gerrity, Jr., J. P., and Nickovic, S.: An Alternative Approach to  
37 Nonhydrostatic Modeling, *Mon. Wea. Rev.*, 129, 1164-1178, 2001.

38 *Janssen, P.A.E.M.:The interaction of ocean waves and wind, Cambridge University*  
39 *Press, ISBN 9780521121040, pp. 385, 2004.*

40 Janssen, P. A. E. M.: Quasi-linear theory of wind-wave generation applied to wave  
41 forecasting, *Journal of Physical Oceanography*, Vol. 21, 1631-1642, 1991.

- 1 Janssen, P. A. E. M.: Wave-induced stress and the drag of air flow over sea waves, *J.*  
2 *Phys. Oceanogr.*, 19(6), 745-754, 1989.
- 3 Kallos, G., Nickovic, S., Papadopoulos, A., Jovic, D., Kakaliagou, O., Misirlis, N.,  
4 Boukas, L., Mimikou, N., Sakellaridis, G., Papageorgiou, J., Anadranistakis, E., and  
5 Manousakis, M.: The regional weather forecasting system SKIRON: An overview, in:  
6 *Proceedings of the Symposium on Regional Weather Prediction on Parallel Computer*  
7 *Environments*, Athens, Greece, 15–17 October 1997, 109-122, 1997.
- 8 Katsafados P., A. Papadopoulos, E. Mavromatidis and I. Pytharoulis: The role of sea  
9 surface temperature in the development of an explosive cyclogenesis: The storm of  
10 21-22 January 2004 in the Eastern Mediterranean. *Nat. Hazard Earth Sys. Sci.*, 11,  
11 1233–1246, doi:10.5194/nhess-11-1233-201, 2011.
- 12 Korres, G., Papadopoulos, A., Katsafados, P., Ballas, D., Perivoliotis, L., and Nittis,  
13 K.: A 2-year intercomparison of the WAM-Cycle4 and the WAVEWATCH-III wave  
14 models implemented within the Mediterranean Sea, *Medit. Mar. Sci.*, 12(1), 129-152,  
15 2011.
- 16 Lionello, P., Martucci, G., Zampieri, M.: Implementation of a Coupled Atmosphere-  
17 Wave-Ocean Model in the Mediterranean Sea: Sensitivity of the Short Time Scale  
18 Evolution to the Air-Sea Coupling Mechanisms, *Glob. Atmos. Ocean Syst.*, Vol. 9,  
19 Iss. 1-2, 65-95, 2003.
- 20 Liu, B., Liu, H., Xie, L., Guan, C., and Zhao, D.: A Coupled Atmosphere-Wave-  
21 Ocean Modeling System: Simulation of the Intensity of an Idealized Tropical  
22 Cyclone, *Mon. Wea. Rev.*, 139, 132-152, 2011.
- 23 Makin, V. K.: A note on the drag of the sea surface at hurricane winds, *Bound Lay.*  
24 *Meteor.*, 115.1, 169-176, 2005.
- 25 Mesinger, F., Janjic, Z. I., Nickovic, S., Gavrilov, D., and Deaven, D. G.: The step-  
26 mountain coordinate: Model description and performance for cases of Alpine lee  
27 cyclogenesis and for a case of an Appalachian redevelopment, *Mon. Wea. Rev.*, 116,  
28 1493-1518, 1988.
- 29 Monbaliu, J., Hargreaves, R., Albiach, J., Luo, W., Sclavo, M., and Günther, H.: The  
30 spectral wave model, WAM, adapted for applications with high spatial resolution,  
31 *Coast. Eng.*, 41, 41-62, 2000.
- 32 Moon, I., Ginis, I., and Hara, T.: Effect of surface waves on Charnock coefficient  
33 under tropical cyclones, *Geophys. Res. Lett.*, 31, L20302, 2004.
- 34 Nickovic, S., Kallos, G., Papadopoulos, A., and Kakaliagou, O.: A model for  
35 prediction of desert dust cycle in the atmosphere, *J. Geophys. Res.*, 106, 18113-  
36 18129, 2001.
- 37 Papadopoulos, A., Katsafados, P., Kallos, G., and Nickovic, S.: The weather  
38 forecasting system for POSEIDON-An overview, *Glob. Atmos. Ocean Syst.*, 8 (2-3),  
39 219-237, 2002.
- 40 Papadopoulos, A. and Katsafados, P.: Verification of operational weather forecasts  
41 from the POSEIDON system across the Eastern Mediterranean, *Nat. Haz. Eart. Syst.*  
42 *Sci.*, 9, 4, pp. 1299-1306, 2009.

- 1 Philander, S. G. H., Pacanowski, R. C., Lau, N. C., and Nath, M. J.: Simulation of  
2 ENSO with a global atmospheric GCM coupled to a high-resolution, tropical Pacific  
3 Ocean GCM. *J. Clim.*, 5(4), 308-329, 1992.
- 4 Redler, R., Valcke, S., and Ritzdorf, H.: OASIS4 - a coupling software for next  
5 generation earth system modeling, *Geosci. Model Dev.*, 3, 87-104, 2010.
- 6 Renault, L., Chiggiato, J., Warner, J. C., Gomez, M., Vizoso, G., and Tintoré, J.:  
7 Coupled atmosphere-ocean-wave simulations of a storm event over the Gulf of Lion  
8 and Balearic Sea, *J. Geophys. Res.*, 117(C09019), 2012.
- 9 Roberts, W. H., and Battisti, D. S.: A new tool for evaluating the physics of coupled  
10 atmosphere-ocean variability in nature and in general circulation models, *Clim. Dyn.*,  
11 36(5-6), 907-923, 2011.
- 12 Sanders, F. and J.R. Gyakum: Synoptic-dynamic climatology of the bomb, *Mon. Wea.*  
13 *Rev.*, 108, 1589-1606, 1980.
- 14 Soden, B. J., and Held, I. M.: An assessment of climate feedbacks in coupled ocean-  
15 atmosphere models, *J. Clim.*, 19(14), 3354-3360, 2006.
- 16 Snir M., Otto, S., Huss-Lederman, S., Walker, D., and Dongarra, J.: MPI-The  
17 complete reference. ISBN 0-262-69215-5, Massachusetts Institute of Technology,  
18 1998.
- 19 Varlas, G., Papadopoulos, A., Korres, G., and Katsafados, P.: Modeling the air-sea  
20 wave interaction processes in an explosive cyclone over the Mediterranean Sea, 12<sup>th</sup>  
21 International Conference on Meteorology, Climatology and Atmospheric Physics  
22 (COMECAP 2014), University of Crete, Heraklion, Crete, Greece, 28-31 May 2014,  
23 Vol. 3, 289-294, 2014.
- 24 Voldoire, A., Sanchez-Gomez, E., Salas y Mélia, D., Decharme, B., Cassou, C.,  
25 Sénési, S., Valcke, S., Beau, I., Alias, A., Chevallier, M., Déqué, M., Deshayes, J.,  
26 Douville, E. Fernandez, G. Madec, E. Maisonnave, M.-P. Moine, S. Planton, D. Saint-  
27 Martin, H., Szopa, S., Tyteca, S., Alkama, R., Belamari, S., Braun, A., Coquart, L.,  
28 Chauvin, F.: The CNRM-CM5.1 global climate model: description and basic  
29 evaluation, *Clim. Dyn.*, vol. 40(9): 2091-2121, 2012.
- 30 Warner, J. C., Armstrong, B., He, R., and Zambon, J. B.: Development of a coupled  
31 ocean-atmosphere-wave-sediment transport (COAWST) modeling system, *Ocean*  
32 *Model.*, 35(3), 230-244, 2010.
- 33

1

2 Table 1: The configuration of the WEW.

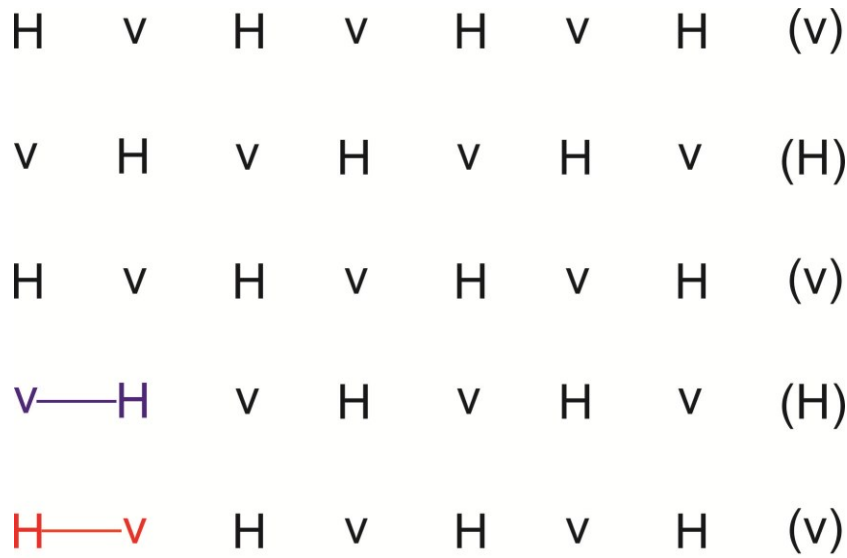
<b>WEW version 5</b>	<b>Atmospheric component</b>	<b>Ocean wave component</b>
Integration domain	Mediterranean Sea, Europe, Black Sea	
Grid	Arakawa semistaggered E grid defined in transformed lat/lon coordinate system	Regular lat/lon coordinate system
Horizontal grid increment	0.05°x0.05°	
Vertical coordinate	Step mountain, $\eta$ coordinate	-
Vertical levels	38	-
Timesteps (sec)	15	120/360
Initial&boundary conditions	ECMWF, 0.5x0.5, 11 isobaric levels, 6hr update of the boundary conditions	Initialization from the atmospheric component, refresh rate every 360 sec
MPI/OMP topology	16 MPI processing threads + 4 I/O servers=20	8 OMP threads

3

4

5

1



H=mass point, v=wind point  
red=(1,1), blue=(1,2)

2

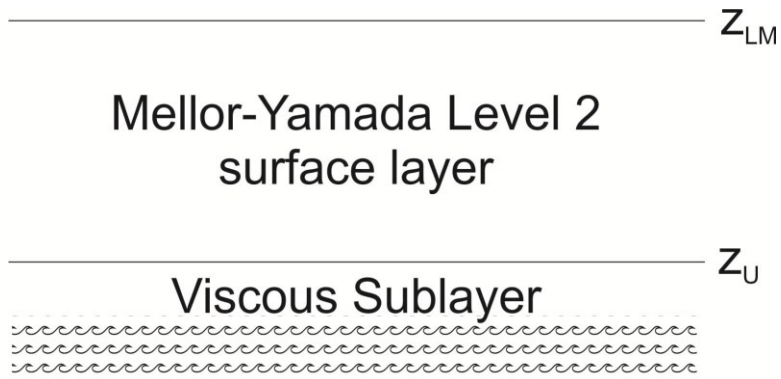
3

4 Figure 1. The E-grid stagger. The mass points represent by H and the wind points  
5 represent by v.

6

7

8

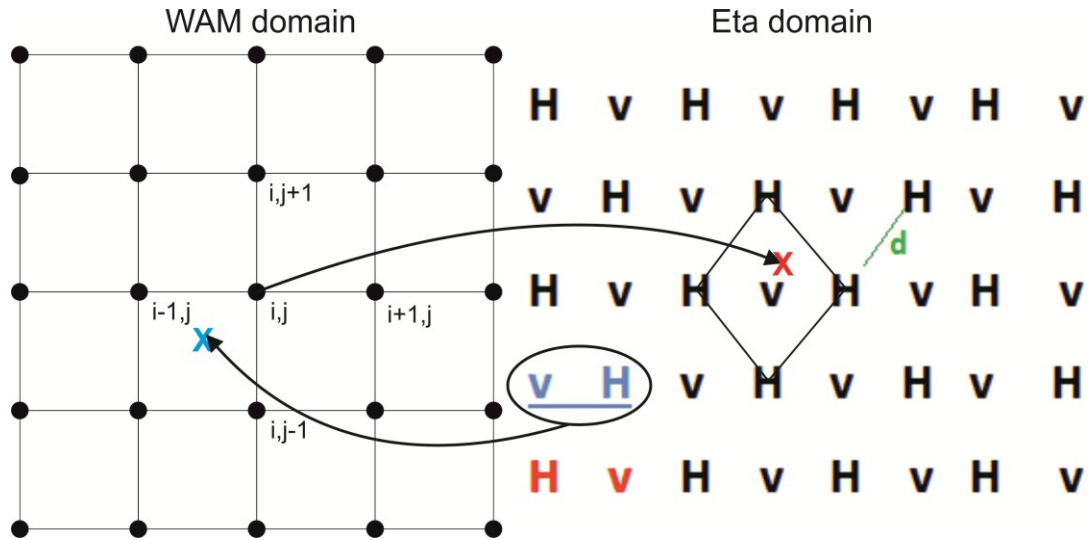


1  
2  
3  
4  
5  
6  
7

Figure 2. The Mellor-Yamada surface layer with the viscous sublayer over the ocean. The symbol  $Z_{LM}$  is the height of the lowest model layer and  $Z_U$  is the depth of the viscous sublayer for momentum. (Reproduced from Janjic, 1994).



1



2

3

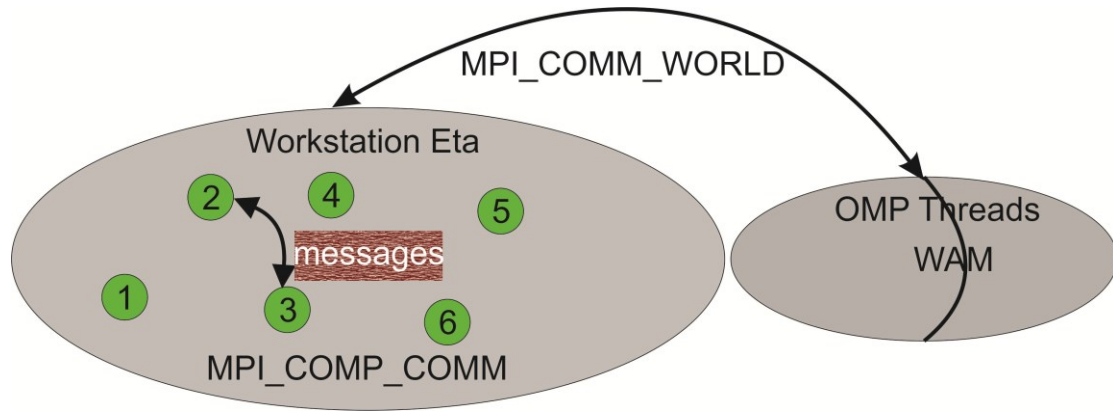
4 Figure 4. Sketch of the WEW multi-grid structure. The transformations from the  
 5 Arakawa-E grid to the regular lat-lon grid and vice versa are also depicted.

6

7

8

1



2

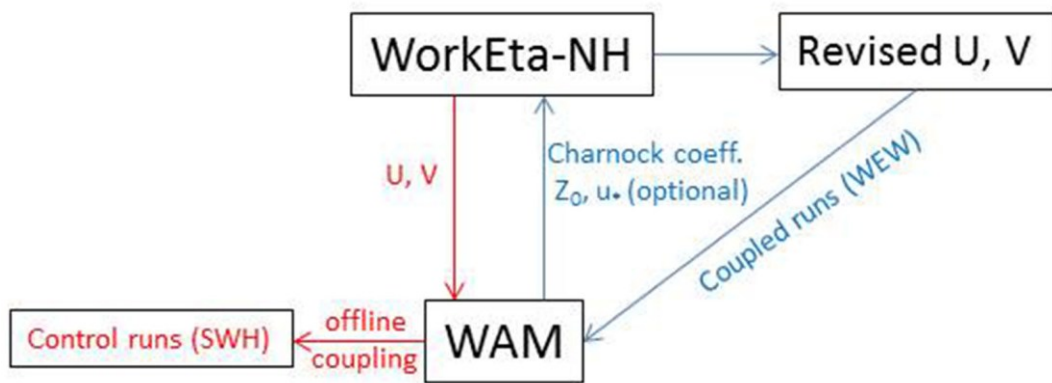
3

4 Figure 5. The WEW intra- and inter-communicators.

5

6

1



2

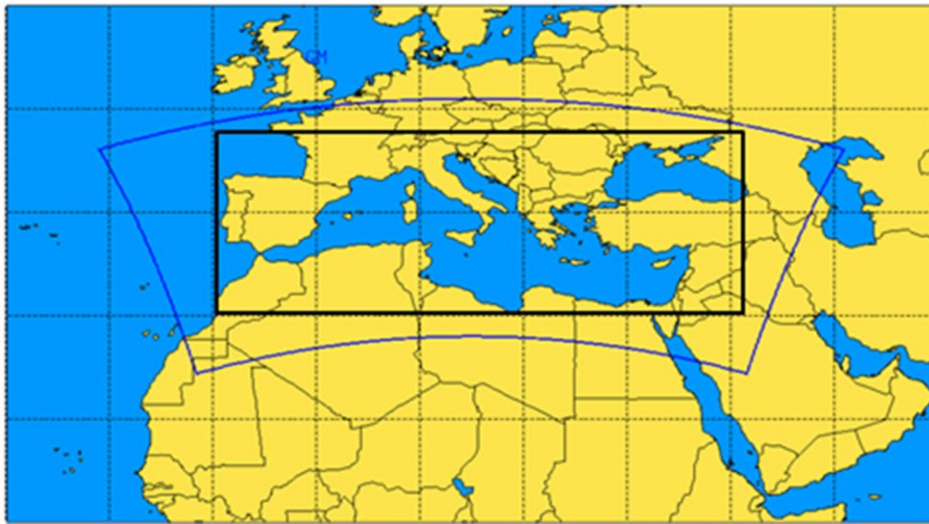
3

4 Figure 6. Informational flowchart for the offline coupled (red lines) and the two-way  
5 coupled simulations (blue lines).

6

7

1



2

3

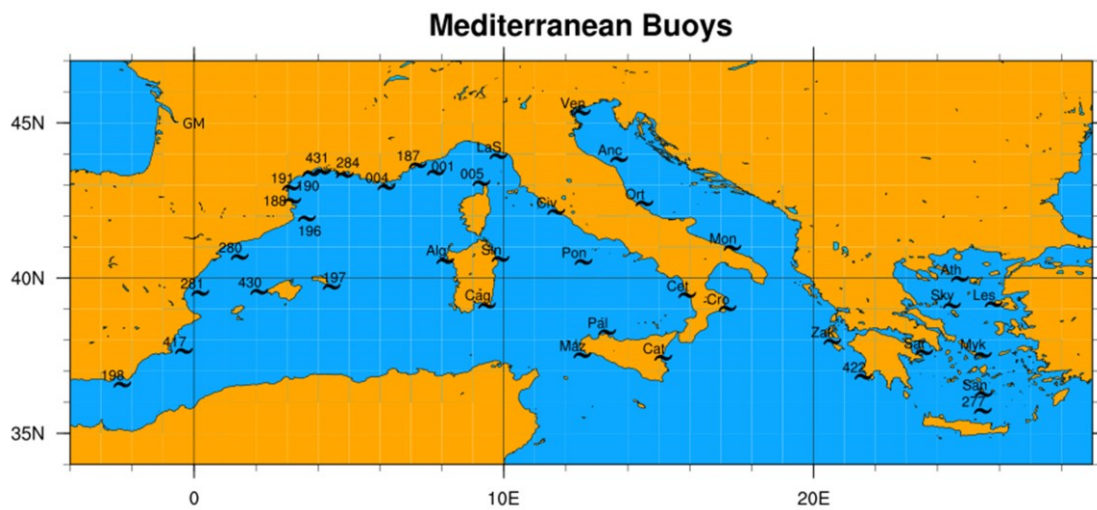
4 Figure 7. Current domains configuration of the atmospheric (blue line) and the ocean-  
5 wave models (black line).

6

7

8

1



2

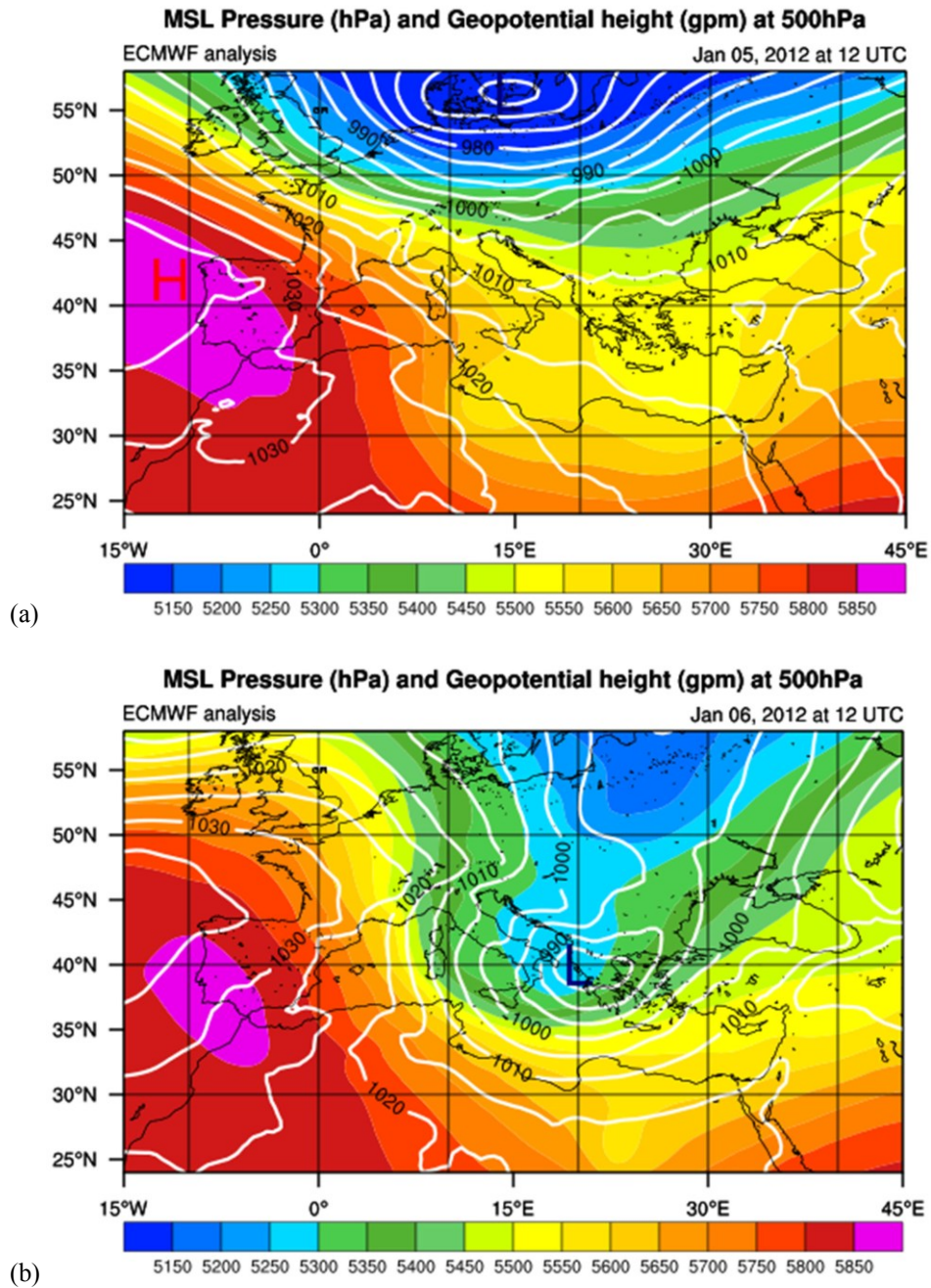
3

4 Figure 8. Spatial distribution of the Mediterranean buoys applied for the sensitivity  
5 test of the system. Data were made available from ISPRA in the framework of  
6 MyWave project.

7

8

1



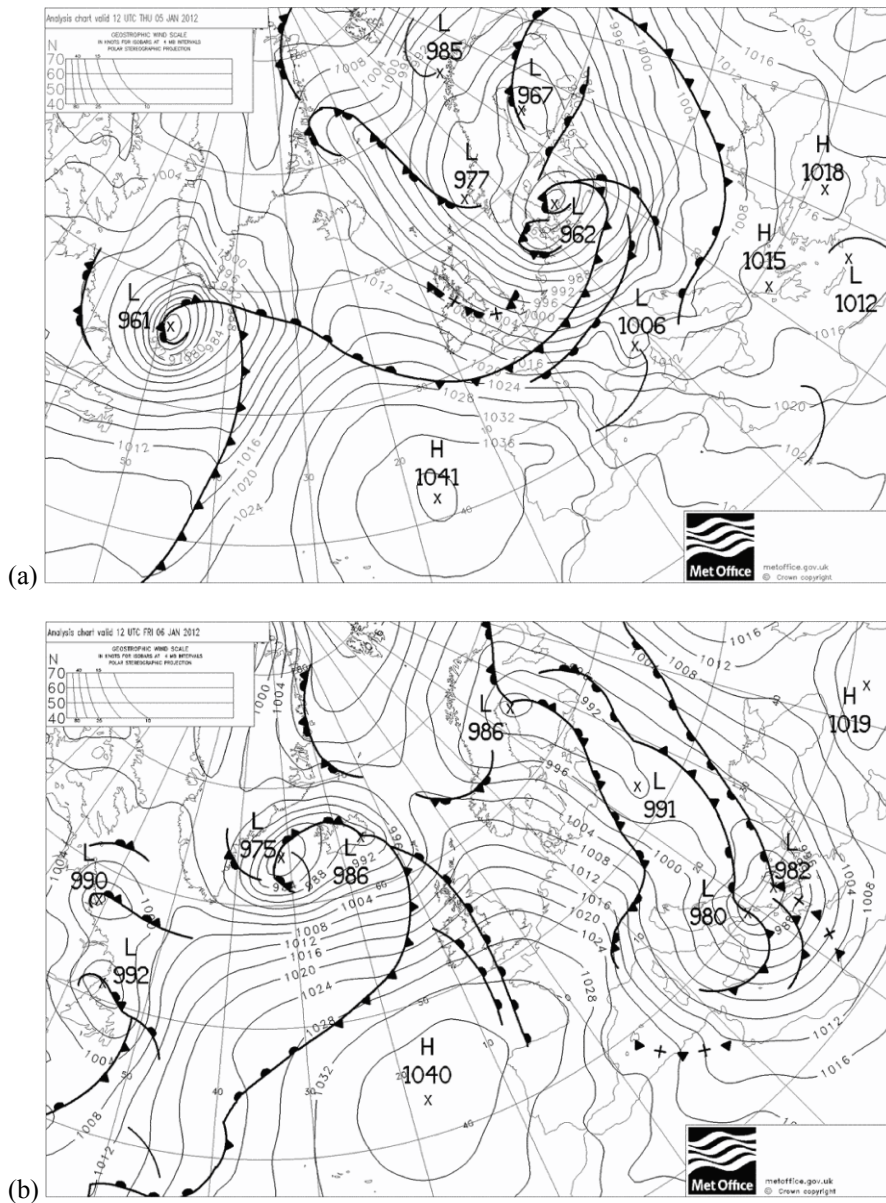
2

3 Figure 9. Mean Sea Level Pressure (contours in hPa) and geopotential height at 500  
4 hPa (colored shaded in gpm) for a) January 5 at 12:00 UTC b) January 6 at 12:00  
5 UTC, 2012. Data are based on ECMWF operational analysis.

6

7

1



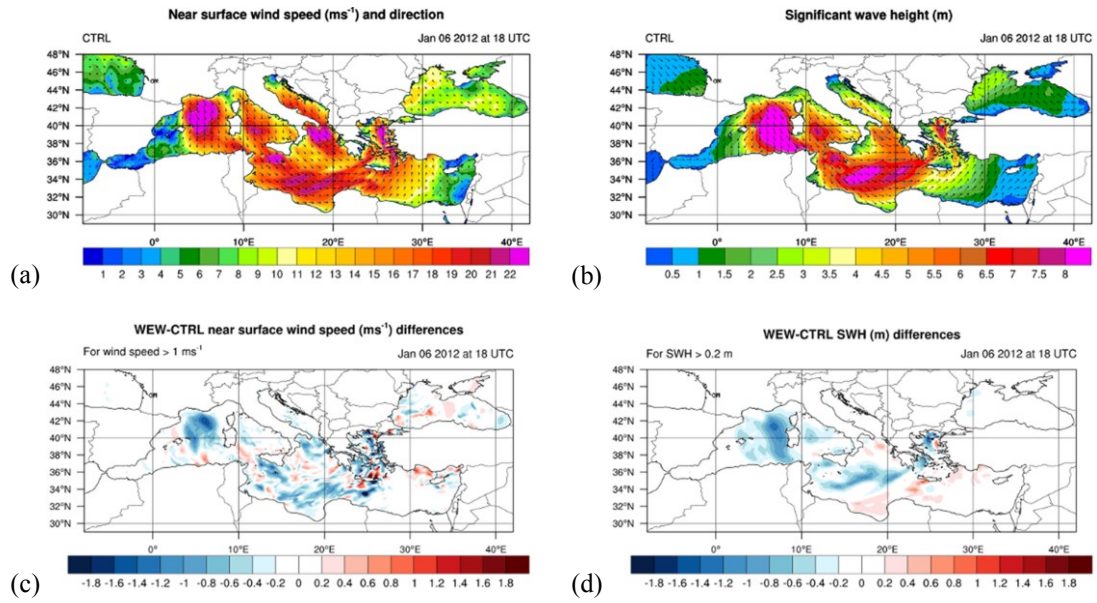
2

3 Figure 10. Surface pressure analysis map (mb) for a) January 5 at 12:00 UTC b)  
4 January 6 at 12:00 UTC, 2012. The maps derived from UK Met office surface  
5 analysis archive.

6

7

1



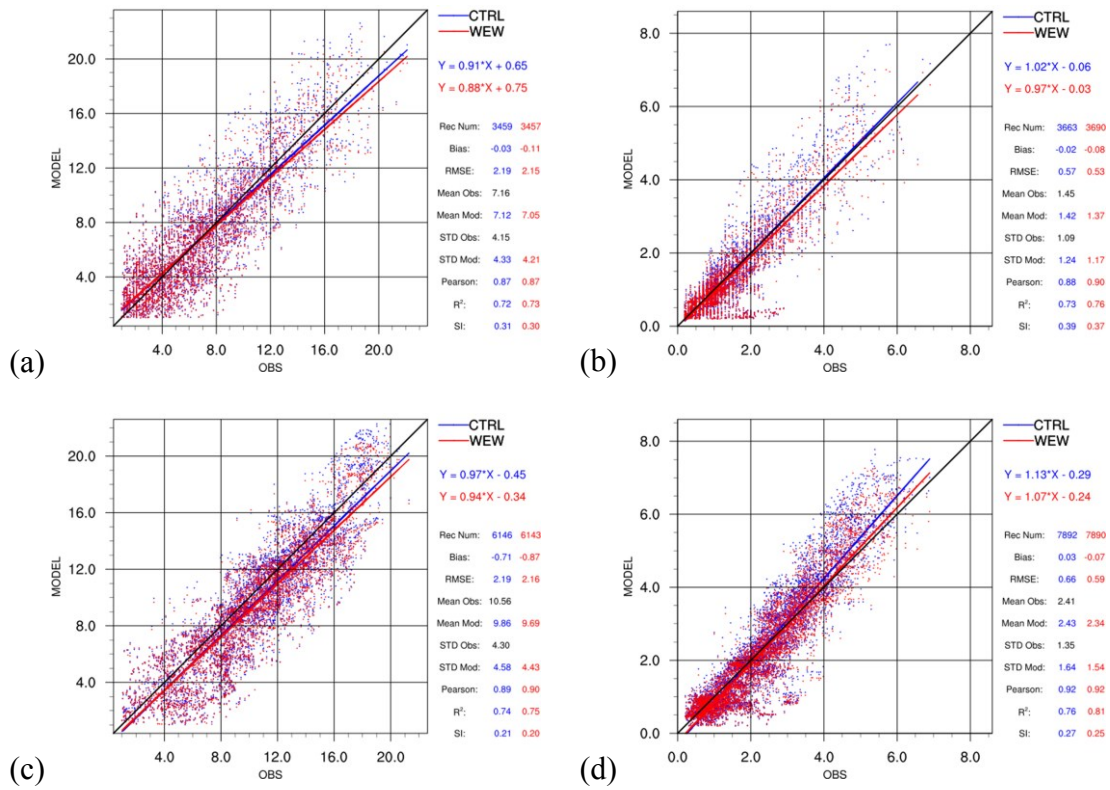
2

3 Figure 11. Panel of the horizontal distribution for the (a) wind speed, (b) SWH and  
4 their differences between WEW and CTRL experiments for the (c) wind speed and  
5 (d) SWH for January 6, 2012 at 18 UTC.

6

7

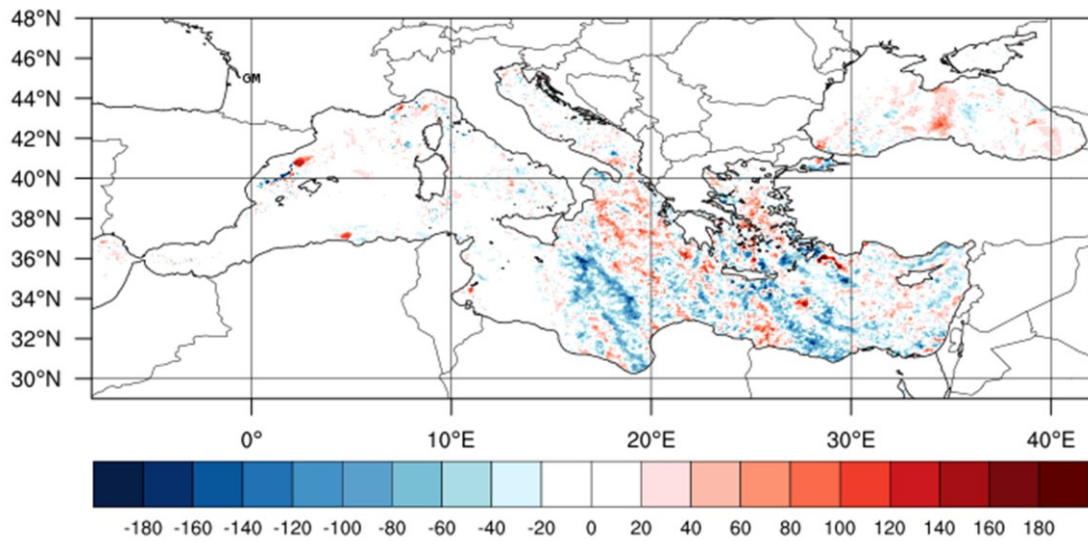
1



2 Figure 12. Scatter plots of the near surface wind speed exceeding 1 ms<sup>-1</sup> (a and c) and  
 3 the significant wave height exceeding 0.2 m (b and d) against the network of the  
 4 Mediterranean buoys (a and b) and the remote sensed retrievals (c and d). Y-axis  
 5 presents the model-estimated values and X-axis the buoys observations (a and b) and  
 6 the satellite estimations (c and d). CTRL and WEW evaluation results are shown in  
 7 blue and red colors respectively.

8  
 9

1



2

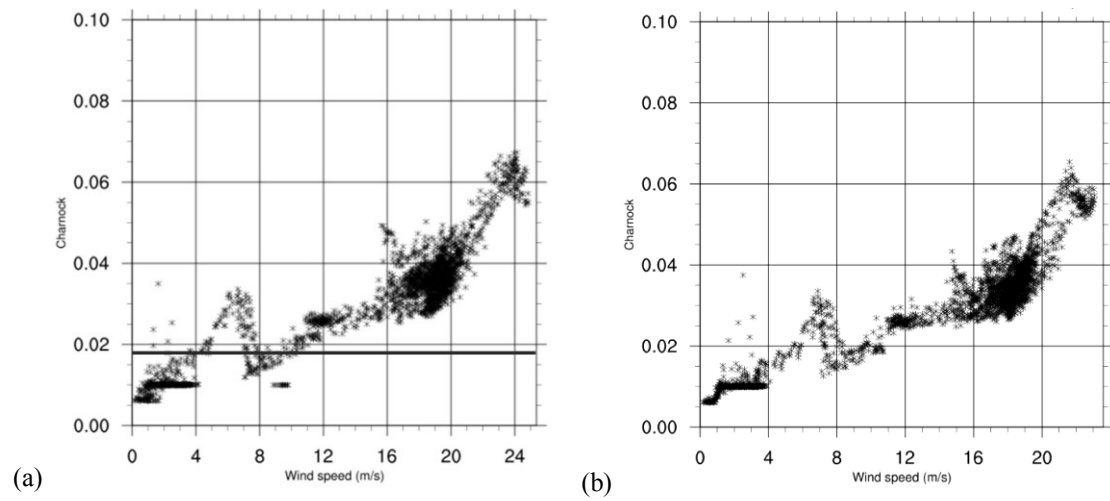
3

4 Figure 13. Spatial distribution of the averaged PBL height (in m) difference (WEW-  
5 CTRL).

6

7

1



2

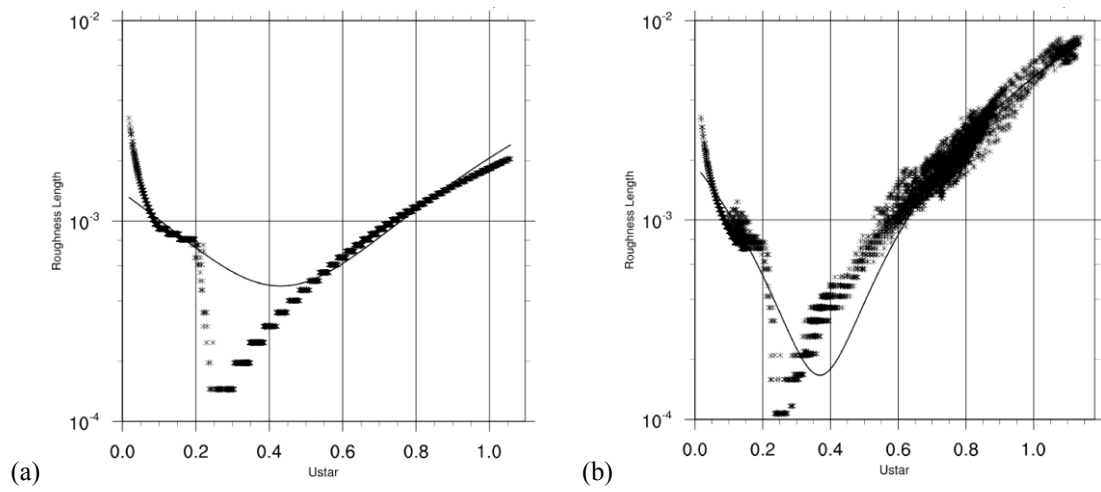
3 Figure 14. Charnock coefficient dependence to the wind speed in (a) offline coupled  
4 simulations. The thick solid line indicates the constant Charnock value (0.018) in the  
5 MYJ surface layer parameterization scheme. (b) WEW simulations.

6

7

8

1



2

3 Figure 15. Roughness length (m) dependence to the friction velocity (ms<sup>-1</sup>) for (a) the  
4 CTRL and (b) WEW experiments.

5